Exome Sequencing Reveals a Homozygous *SYT14* Mutation in Adult-Onset, Autosomal-Recessive Spinocerebellar Ataxia with Psychomotor Retardation

Hiroshi Doi,[1,2] Kunihiro Yoshida,[3] Takao Yasuda,[4] Mitsunori Fukuda,[4] Yoko Fukuda,[5] Hiroshi Morita,[6] Shu-ichi Ikeda,[6] Rumiko Kato,[7] Yoshinori Tsurusaki,[1] Noriko Miyake,[1] Hirotomo Saitsu,[1] Haruya Sakai,[1] Satoko Miyatake,[1] Masaaki Shiina,[8] Nobuyuki Nukina,[9] Shigeru Koyano,[2] Shoji Tsuji,[5] Yoshiyuki Kuroiwa,[2] and Naomichi Matsumoto[1,*]

Autosomal-recessive cerebellar ataxias (ARCAs) are clinically and genetically heterogeneous disorders associated with diverse neurological and nonneurological features that occur before the age of 20. Currently, mutations in more than 20 genes have been identified, but approximately half of the ARCA patients remain genetically unresolved. In this report, we describe a Japanese family in which two siblings have slow progression of a type of ARCA with psychomotor retardation. Using whole-exome sequencing combined with homozygosity mapping, we identified a homozygous missense mutation in *SYT14*, encoding synaptotagmin XIV (SYT14). Expression analysis of the mRNA of *SYT14* by a TaqMan assay confirmed that *SYT14* mRNA was highly expressed in human fetal and adult brain tissue as well as in the mouse brain (especially in the cerebellum). In an in vitro overexpression system, the mutant SYT14 showed intracellular localization different from that of the wild-type. An immunohistochemical analysis clearly showed that SYT14 is specifically localized to Purkinje cells of the cerebellum in humans and mice. Synaptotagmins are associated with exocytosis of secretory vesicles (including synaptic vesicles), indicating that the alteration of the membrane-trafficking machinery by the *SYT14* mutation may represent a distinct pathomechanism associated with human neurodegenerative disorders.

Hereditary ataxias are genetically heterogeneous neurological disorders: autosomal-dominant, autosomal-recessive, X-linked, and mitochondrial types are known. Among ataxias, spinocerebellar ataxia (SCA) is relatively common and involves the cerebellum, brainstem, or spinocerebellar long tracts.[1] Autosomal-recessive cerebellar ataxias (ARCAs) are generally associated with diverse neurological and nonneurological attributes, resulting in complex phenotypes. ARCAs include congenital nonprogressive ataxias and progressive ataxias such as SCAs.[2] The clinical onset of ARCAs usually occurs before the age of 20, even if congenital types are excluded.[1,3,4] Currently, more than 20 defective genes have been identified in ARCAs.[2,5,6] These genes have variable recognized functions, including those involving mitochondrial energy generation, cellular metabolisms, DNA repair, chaperone-mediated protein folding, RNA processing, and ion channels.[1,3,6] Approximately half of the patients with ARCAs remain genetically unresolved.[4] Therefore, more investigations of ARCAs are required. In this study, we describe a Japanese family with two siblings showing psychomotor retardation and the slowly progressive type of SCA without involvement of pyramidal tracts or peripheral nerves. Exome sequencing combined with homozygosity mapping successfully identified a causative mutation.

Clinical information and blood materials were obtained from the family members after written informed consent was secured. Experimental protocols were approved by IRBs of the Yokohama City University and the Shinshu University. Among the children of first-cousin parents, two siblings (IV-3 and IV-4) were found to be affected, whereas the other two (IV-1 and IV-2) were healthy (Figure 1A). No similar patients were recognized within the family. IV-3 had mild psychomotor retardation from childhood. He found a job after graduating from an ordinary junior high school. At 35 years of age, he lost his job for social reasons. Although he had some gait disturbances from childhood, he could independently go shopping and walk a dog even after leaving his occupation. At the age of ~56, he developed obvious gait unsteadiness and began to stumble frequently. At 58, he started to choke on food. These symptoms gradually worsened, and he sought medical examination at 59 years of age. He displayed disturbances of smooth-pursuit eye movements, dysarthria, mild limb ataxia, and moderate truncal ataxia. His muscle tone was normal, and no involuntary

[1]Department of Human Genetics, Graduate School of Medicine, Yokohama City University, 3-9 Fukuura, Kanazawa-ku, Yokohama 236-0004, Japan; [2]Department of Clinical Neurology and Stroke Medicine, Graduate School of Medicine, Yokohama City University, 3-9 Fukuura, Kanazawa-ku, Yokohama 236-0004, Japan; [3]Division of Neurogenetics, Department of Brain Disease Reseach, Shinshu University School of Medicine, 3-1-1 Asahi, Matsumoto, Nagano 390-8621, Japan; [4]Laboratory of Membrane Trafficking Mechanisms, Department of Developmental Biology and Neuroscience, Graduate School of Life Sciences, Tohoku University, Aobayama, Aoba-ku, Sendai, Miyagi 980-8578, Japan; [5]Department of Neurology, Graduate School of Medicine, The University of Tokyo, 7-3-1 Hongo, Bunkyo-ku, Tokyo 113-8655, Japan; [6]Department of Medicine (Neurology & Rheumatology), Shinshu University School of Medicine, 3-1-1 Asahi, Matsumoto, Nagano 390-8621, Japan; [7]Department of Pediatrics, National Higashi-Saitama Hospital, 4147 Kurohama, Hasuda 349-0196, Japan; [8]Department of Biochemistry, Graduate School of Medicine, Yokohama City University, 3-9 Fukuura, Kanazawa-ku, Yokohama 236-0004, Japan; [9]Laboratory for Structural Neuropathology, Brain Science Institute, RIKEN, 2-1 Hirosawa, Wako 351-0198, Japan
*Correspondence: naomat@yokohama-cu.ac.jp
DOI 10.1016/j.ajhg.2011.07.012.

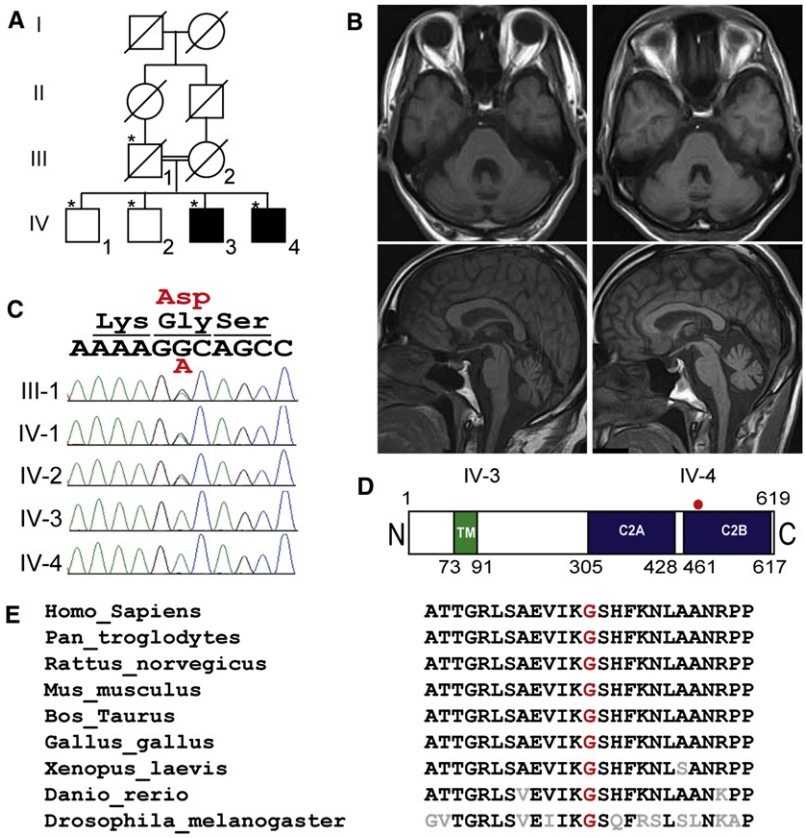

Figure 1. Familial Pedigree, Brain MRI of Patients, and the *SYT14* Mutation Identified

(A) Familial pedigree of the patients with autosomal-recessive spinocerebellar ataxia. *An asterisk indicates members whose genomic DNA was available for this study.

(B) Brain MRI of IV-3 at 59 years of age (left panels) and IV-4 at 56 years of age (right panels). Axial (upper panels) and sagittal (lower panels) sections of a T1-weighted image are shown.

(C) Electropherograms of unaffected (III-1, IV-1, and IV-2) and affected (IV-3 and IV-4) members, who show the mutation.

(D) Schematic presentation of SYT14. The red dot indicates the location of the mutation in the C2B domain.

(E) The missense mutation occurred at an evolutionarily conserved amino acid (in red).

movements were observed. Laboratory examination, including analysis of serum albumin, vitamin E, and α-fetoprotein, was normal. A nerve-conduction study (NCS) indicated no neuropathy. No retinitis pigmentosa was recognized by ophthalmologic evaluation. Brain magnetic resonance imaging (MRI) revealed mild atrophy of the cerebellar vermis and hemispheres but no apparent atrophy of the brain stem or the cerebral cortex. (Figure 1B, left panels).

Similar to IV-3, IV-4 also had psychomotor retardation from childhood, but this retardation was more severe than that of IV-3. After graduation from a school for disabled children at the age of 15, he entered a facility for disabled people. He showed gait disorder, but he was able to walk without a cane. At an age of ~50, his gait disturbance worsened, and he went for a medical check at a hospital when he was 56 years old. He displayed disturbance of smooth-pursuit eye movements, gaze-evoked horizontal nystagmus, dysarthria, mild limb ataxia, and moderate truncal ataxia. No involuntary movements were observed. His laboratory tests, including those for serum albumin, vitamin E, and α-fetoprotein, were normal. NCS was normal. A brain MRI was similar to that of IV-3 (Figure 1B, right panels). The clinical manifestations of these two patients are summarized in Table 1.

To search for the disease locus, we conducted genome-wide SNP genotyping of III-1, IV-1, IV-2, IV-3, and IV-4 by using the Genome-wide Human SNP Array 6.0 (SNP 6.0 array) (Affymetrix, Inc., Santa Clara, CA) according to the manufacturer's instructions. Then, SNP 6.0 array data were subjected to homozygosity mapping with HomozygosityMapper software.[7] For the linkage analysis, a subset of 7339 SNPs with high heterozygosity (mean heterozygosity 0.49) was extracted from the SNP 6.0 array data with the program Linkdatagen, for which the bin size was set to 0.5cM and the allele frequency of the Japanese population was used.[8] The multipoint LOD score was calculated with Allegro version 2[9] on the basis of the model of autosomal-recessive and X-linked-recessive inheritance, respectively. In both models, complete penetrance and a disease-allele frequency of 0.0001 were adopted. The homozygosity mapping revealed a total of three regions, which together were approximately 11.35 Mb in size, as candidate loci, where genes known to be mutated in ARCA did not exist (Table 2). In the model of autosomal-recessive inheritance, a total of ten regions with a LOD score greater than 1.5 in the multipoint linkage analysis were identified (Table S1). The three homozygous regions in accordance with the linked regions still survived as candidate regions. On the basis of X-linked recessive inheritance, a total of three regions with positive LOD scores (maximum LOD score = 0.9031) were highlighted; together, these three regions were approximately 101.03 Mb (Table S1).

To find a gene mutation within the candidate loci, we performed whole-exome sequencing on IV-3 and IV-4. Three micrograms of genomic DNA was processed with the SureSelect Human All Exon Kit v.1 (approximately 180,000 exons covering 38 Mb of the CCDS database) (Agilent Technologies, Santa Clara, CA) according to the manufacturer's instructions. Captured DNAs were sequenced on an Illumina GAIIx (Illumina, San Diego, CA) with 76 bp pair-end reads. Of the possible eight lanes of the flow cell, two lanes for IV-3 and three lanes for IV-4 (Illumina) were used. Image analysis and base calling

Table 1. Clinical Features of the Patients

Clinical Features	IV-3	IV-4
Age at present	61	58
Sex	male	male
Age of obvious ataxia	56	around 50
Mental retardation	mild	moderate
Ocular apraxia	no	no
Ophthalmoplegia	no	no
Nystagmus	no	+
Dysarthria	+	+
Truncal ataxia	++	++
Limb ataxia	+	+
Extrapyramidal signs	no	no
Involuntary movements	no	no
Sensory involvements	no	no
Tendon reflex	normal-increased	normal-decreased
Plantar responses	normal	normal
Peripheral neuropathy	no	no
Pes cavus	no	no
SARA[a]	12/40	15/40
Cerebellar atrophy on MRI	+	+
others	normal level of serum albumin, vitamin E, and α-fetoprotein	normal level of serum albumin, vitamin E, and α-fetoprotein

[a] SARA: Scale for the assessment and rating of ataxia.[32]

Table 2. Regions of Homozygosity

Chromosome	Chromosomal Position (rsID)	Size (Mb)	LOD
1	207226930 (rs2761781)–213992561 (rs1857229)	6.77	2.0537
4	181929079 (rs918401)–185188999 (rs7690914)	3.26	2.0554
22	45676443 (rs3905396)–47003473 (rs2013591)	1.33	2.0545

Regions of homozygosity were identified by HomozygosityMapper, and the LOD scores were calculated by multipoint linkage analysis, for which SNPs were extracted from SNP 6.0 array data via Linkdatagen.

were performed by sequence control software (SCS) real-time analysis (Illumina) and CASAVA software v1.6 (Illumina). Reads were aligned to the human reference genome sequence (UCSC hg18, NCBI build 36.1) via the ELAND v2 program (Illumina). Coverage was calculated statistically with a script created by BITS (Tokyo, Japan). Approximately 71 million reads from IV-3 and 148 million reads from IV-4 (these numbers of reads passed quality-control [Path Filter]) were mapped to the human reference genome with Mapping and Assembly with Qualities (MAQ)[10] and NextGENe software v2.00 (SoftGenetics, State College, PA) under the default settings. MAQ aligned 59,491,138 and 126,159,746 reads to the whole genome for IV-3 and IV-4, respectively. A script created by BITS was used for extraction of SNPs and indels from the alignment data; dbSNP build 130 served as a reference for registered SNPs. A consensus quality score of 40 or more was adopted for the SNP analysis in MAQ. Coverage analysis revealed that 65.0% (IV-3) and 71.3% (IV-4) of the coding sequences (CDS) were completely covered (100%), and 77.7% (IV-3) and 80.3% (IV-4) of CDS were mostly covered by reads (90% or more) through the whole genome. 79.0% (IV-3) and 79.7% (IV-4) of total CDS were covered by ten reads or more (50 reads or more in 66.4% and 77.1%, respectively).

To identify the pathogenic mutation, we adopted a prioritization scheme, which has been used in recent studies.[11–13] First, we excluded the variants registered in dbSNP130 from all the detected variants and then picked up homozygous mutations and variants in coding regions and the intronic regions within 50 bp from coding sequences. Of the homozygous mutations and variants, we focused on those within the candidate regions. As a result, only two missense mutations or variants, p.Gly484Asp (c.1451G>A) (NM_001146261.1) in exon 8 of *SYT14* (1q32.2, [MIM 610949]) and p.Gln4203Arg (c.12608A>G) (NM_206933.2) in exon 63 of *USH2A* (1q41, [MIM 608400]) remained as candidates for both cases (Table S2). Sanger sequencing with ABI 3500xL (Life Technologies, Carlsbad, CA) confirmed that the c.1451G>A of *SYT14* was homozygous in IV-3 and IV-4 and heterozygous in III-1 (father), IV-1, and IV-2, whereas the c.12608A>G of *USH2A* was homozygous in IV-2 as well as IV-3 and IV-4 (Figure 1C and data not shown). The *SYT14* missense mutation occurred at an evolutionarily conserved amino acid among different species and resides in the second C2 (C2B) domain (Figures 1D and 1E). In silico analysis incorporating different tools, including Polyphen, Polyphen2, SIFT, and Align GVGD, consistently indicated that the change was damaging (Table S3). The mutation was not detected in 576 Japanese control chromosomes, indicating that the mutation is very rare. On the basis of the X-linked recessive model, no pathological hemizygous mutation of protein-coding genes was detected in the possible candidate loci (Table S4).

We considered the *SYT14* mutation to be the causative agent and used the Sanger method to conduct mutation screening of all the coding regions of *SYT14* in 65 simplex SCA cases and 37 SCA familial cases, including three with autosomal-recessive inheritance. Only p.Gly183Glu (c.548G>A) was found in one family with autosomal-dominant SCA; however, the change was not consistent with the SCA phenotype in the family (Table S3). Thus, we could not detect any other pathological changes in *SYT14*. This was probably due to the small number of cases tested.

Synaptotagmin XIV (SYT14), which is encoded by *SYT14*, is a member of the synaptotagmins (SYTs), which are membrane-trafficking proteins, and SYT14 is conserved across many organisms.[14] Although the original report indicated that *SYT14* was not expressed in mouse brain,[14] multiple lines of evidence, including from the Allen brain Atlas, suggest that *SYT14* is expressed in the central nervous system (CNS) of the fly, mouse, and human brains.[15,16] To confirm *SYT14* expression in the CNS, we performed TaqMan quantitative real-time PCR analysis with cDNAs of adult human tissue (Human MTC Panel I, #636742) (Clontech Laboratories, Mountain View, CA), fetal human tissue (Human Fetal MTC Panel, #636747) (Clontech Laboratories), mouse tissue (Mouse MTC Panel I, #636745) (Clontech Laboratories), and various regions of the mouse brain (GSMBRSET) (NIPPON Genetics, Tokyo, Japan) as templates. Predesigned TaqMan probe sets for human *SYT14* (Hs00950169_m1), mouse *Syt14* (Mm00805319_m1), human *β-actin* (*ACTB*, 4326315E), and mouse *Actb* (43522341E) from Applied Biosystems were used. PCR reactions (total volume of 20 μl) contained 10 μl of the TaqMan Gene Expression Master Mix (Applied Biosystems), 1 μl of 20 × TaqMan reagents for *ACTB/Actb* and *SYT14/Syt14*, and 1 μl of cDNA (containing 1 ng cDNA in MTC panels and 25 ng cDNA in GSMBRSET) as the template. PCR was performed on a Rotor-Gene Q (QIAGEN, Valencia, CA) as follows: 2 min at 50°C and 10 min at 95°C, then 40 cycles of 95°C for 15 s and 60°C for 1 min. Expression levels were calculated with the Rotor-Gene Q Series Software (QIAGEN) by the $2^{-\Delta\Delta Ct}$ method. The cycling threshold (Ct) of the target gene was compared with the Ct of *ACTB* cDNA, and ΔCt was expressed as Ct of *SYT14* − Ct of *ACTB*. ΔΔCt was expressed as ΔCt of the control sample − ΔCt of each sample, and relative concentration was determined as $2^{-\Delta\Delta Ct}$. Expression in the kidney and the cerebral cortex was used as the control in Figures 2A–2D. *SYT14* was predominantly expressed in human adult and fetal brain tissues (Figures 2A and 2B). Even in mice, substantial expression in the brain was confirmed (but, not predominant) (Figure 2C). Among various brain regions in mice, *SYT14* was mostly expressed in the cerebellum (Figure 2D).

Intracellular distribution of SYT14 in cultured cells was investigated. The full-length *SYT14* PCR product amplified from human brain cDNA (MHS4426-99239810, Open Biosystems, Huntsville, AL) was used as a template and subcloned into pDONR221 (the entry vector of Gateway system, Invitrogen). We used site-directed mutagenesis to produce the *SYT14* mutant and variants by using a mutagenesis kit (Toyobo, Osaka, Japan). Variants include c.611C>T and c.810_812del, which are registered in dbSNP130, and c.548G>A, which was detected in an SCA patient with autosomal-dominant inheritance but did not segregate with the phenotype, indicating that it is nonpathogenic (Table S3). All constructs were verified by DNA sequencing. Each construct was recloned into the pEF-DEST51 mammalian expression vector (Invitrogen) and transfected to COS-1 cells with the FuGENE^{R}6 transfection reagent (Roche Applied Science, Mannheim, Germany) according to the manufacturer's instructions. Localization of the mutant (p.Gly484Asp) was clearly different from that of the wild-type and other (normal) variants. Whereas the wild-type and other variants were localized to the perinuclear and submembranous regions, p.Gly484Asp was localized in the cytoplasm (significant amounts were in the perinuclear region) but formed a characteristic reticular pattern without showing any submembranous distribution (Figures 2E and S2B). Confocal microscopic analysis showed that the p.Gly484Asp mutant was colocalized with an endoplasmic reticulum (ER) marker, protein disulfide isomerase (PDI), throughout the cells, whereas the wild-type colocalized with PDI dominantly in perinuclear regions (Figure 2F). immunoblot analysis combined with subcellular fractionation of the transfected cells further confirmed that the mutant was distributed differently from the wild-type. The wild-type and the mutant (p.Gly484Asp) were distributed in the nucleus and Golgi apparatus fractions; however, only the mutant was detected in microsome fractions containing ER fragments together with an ER membrane marker, calnexin (Figure S1).[17] These data suggest that improper folding of the mutant protein results in abnormal retention in the ER.

To investigate the effect of the p.Gly484Asp mutation in the C2B domain on phospholipid binding activity, we amplified cDNA of C2B domains from the wild-type and the p.Gly484Asp mutant from SYT14-expressing vectors by using the following primers: sense, 5′-GGATCCGAAA GTACATCCTCATGTCA-3′; and antisense, 5′-TCATGAC TCTAGCAACGCAT-3′. We then recloned the cDNA into *Escherichia coli* (*E. coli*) expressing vector (pGEX-4T-3). The C2B domain of SYT14 fused to glutathione S-transferase (GST) was expressed in *E. coli* JM109 and purified by standard protocols. Both GST-SYT14-C2B (WT) and GST-SYT14-C2B (p.Gly484Asp) could be mostly purified of contamination by degradation products, but the amount of GST-SYT14-C2B (p.Gly484Asp) obtained was at least four times smaller than that of GST-SYT14-C2B (WT) (data not shown). Liposome (phosphatidylcholine and phosphatidylserine, 1:1, w/w) cosedimentation assay with purified GST-SYT14-C2B was performed as described previously.[18] The result showed that the SYT14-C2B (p.Gly484Asp) bound liposomes similarly to SYT14-C2B (WT) (Figure 2G), indicating that the p.Gly484Asp mutation had no effect on the Ca^{2+}-independent phospholipid-binding activity of the SYT14-C2B domain.

The Allen Mouse Brain Atlas indicates that *Syt14* is expressed in Purkinje cells of the cerebellum in mice; however, SYT14 localization has not been fully investigated.[15] A rabbit polyclonal anti-SYT14 antibody (Ab-SYT14) was generated for immunoblotting and immunocytochemistry (Operon Biotechnologies, Tokyo, Japan) (Figure S2). Immunohistochemical analysis of mouse and human brains was

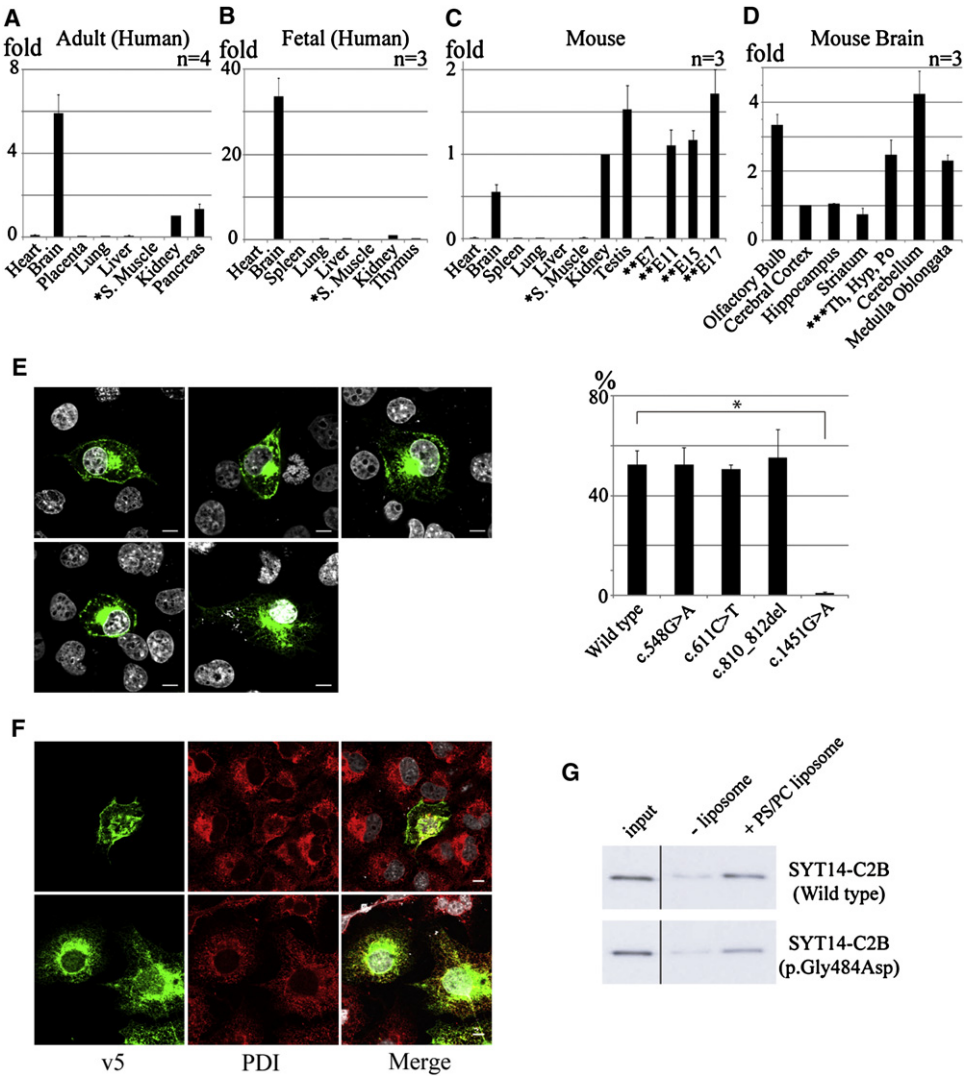

Figure 2. Expression Studies of *SYT14/Syt14* cDNA in Human and Mouse Tissues and Localization of SYT14 in Transfected COS-1 Cells

(A–D) The results of a TaqMan quantitative real-time PCR assay in which the first-strand cDNA of human adult tissues (A), human fetal tissues (B), mouse tissues (C), and various regions of mouse brain (D) were used as templates. The relative cDNA concentrations were determined from cDNA concentrations of the kidney (human adult tissues, human fetal tissues, and mouse tissues) or cerebral cortex (various regions of the mouse brain). Error bars represent the standard deviation. *S. Muscle indicates skeletal muscle. **E7, **E11, **E15, and **E17 indicate mouse embryos at 7, 11, 15, and 17 days of embryonic development, respectively. ***Th, Hyp and Po indicate thalamus, hypothalamus, and pons.

(E) Immunocytochemistry of COS-1 cells transfected with expression vectors of v5/His-tagged wild-type (upper left), p.Gly183Glu (c.548G>A) (upper middle), p.Pro203Leu (c.611C>T) (upper right), p.Glu270del (c.810_812del) (lower left), or p.Gly484Asp (c.1451G>A) (lower middle) SYT14. The SYT14 was detected with the anti-v5 antibody (Alexa fluor 488 as the secondary antibody). Nuclei were stained (white) with 4′,6-diamidino-2-phenylindole (DAPI). The horizontal bars indicate 10 μm. The bar graph indicates the ratio of the cells in which overexpressed proteins were accumulated in submembranous regions. A total of 120 cells per each transfectant in triplicated experiments were counted. Submembranous localization of the mutant (p.Gly484Asp) was mostly unseen, in contrast to the wild-type (*$p < 0.001$).

(F) Immunocytochemical analysis of COS-1 cells transfected with expression vectors of v5/His-tagged wild-type (upper panels) or the p.Gly484Asp mutant (lower panels). The SYT14 was detected with the anti-v5 antibody (Alexa fluor 488 as the secondary antibody), and PDI (protein disulfide isomerase) was visualized with an anti-PDI antibody (Alexa fluor 546 as the secondary antibody). Nuclei were stained (white) with DAPI. The scale bar represents 10 μm. The anti-v5 and anti-PDI antibodies and the Alexa-488-conjugated secondary antibody were all used at a dilution of 1:1000.

(G) Phospholipid binding activity of the C2B domain of the wild-type SYT14 and the p.Gly484Asp mutant. Liposomes and GST-fusion proteins (2 μg) were incubated in 50 mM HEPES-KOH (pH 7.2) in the presence of 2 mM EGTA for 15 min at room temperature. After centrifugation at 12,000 × *g* for 10 min, the supernatants (non-binding fraction) and pellets (phospholipid-binding fraction) were separated as described previously.[18] The pelleted samples and input samples (100 ng) were subjected to 10% SDS-PAGE followed by immunoblotting with horseradish peroxidase-conjugated anti-GST antibody (Santa Cruz Biotechnology, Santa Cruz, CA).

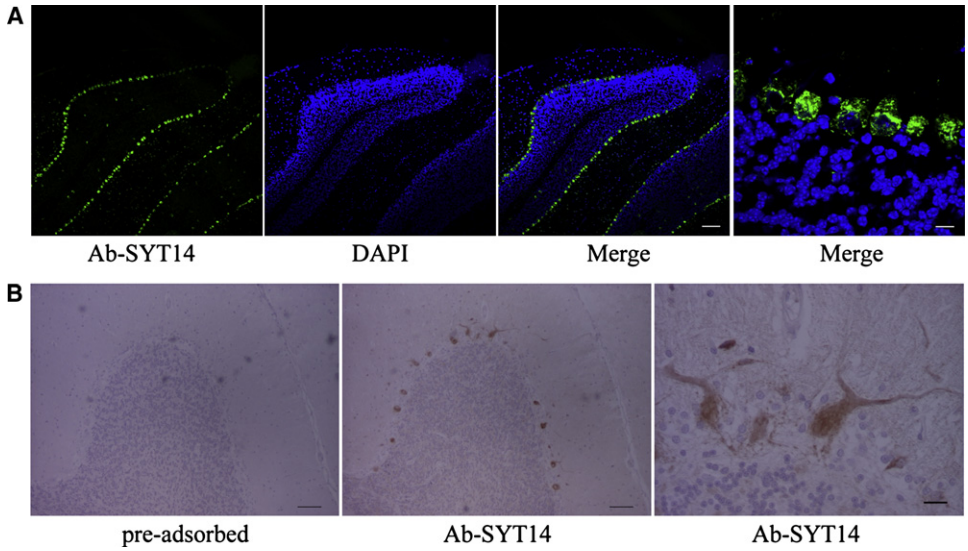

Figure 3. Selective Localization of SYT14 in Purkinje Cells of the Cerebellum in Mice and Humans
(A) Immunohistochemical analysis with the Ab-SYT14 antibody of the cerebellum from an adult mouse at 12 weeks of age. Nuclei were stained with DAPI (the scale bar represents 100 μm). A magnified image is shown in the first right panel (the scale bar represents 10 μm).The Ab-SYT14 antibody (0.9 mg/dl) was used at a dilution ration of 1:2000, and the Alexa-488-conjugated secondary antibody dilution was 1:1000.
(B) Immunohistochemical analysis with the Ab-SYT14 antibody of the cerebellum from the human control. Ab-SYT14 antibodies were preincubated with (left panel) or without (middle panel) peptide antigen before immunostaining. Nuclei were stained with hematoxylin (scale bars represent 100 μm). A magnified image is shown in the right panel (the scale bar represents 20 μm). The Ab-SYT14 antibody (0.9 mg/dl) was used at a dilution of 1:500.

performed with Ab-SYT14, as previously described.[19–21] Mouse brain sections were prepared at the RIKEN Brain Science Institute. Mouse experimental protocols were approved by the animal experiment committee of the RIKEN Brain Science Institute. The frozen brain of C57BL/6J mouse was mounted in Tissue-Tek and sliced to 10 μm sections with a freezing microtome. A human adult brain specimen was obtained through the postmortem examination of a brain from a control subject without neurodegenerative disorders. Informed consent was obtained from the family on the basis of the IRB-approved protocol of Yokohama City University School of Medicine. The human brain was fixed in 10% formalin and cut into 1-cm-thick slices. Sliced tissues were embedded in paraffin wax, and 5 μm sections were immunostained with primary antibodies and visualized with the Vectastain ABC kit (Vector Laboratories, Burlingame, CA). Selective localization of SYT14/Syt14 in Purkinje cells of the mouse cerebellum (Figure 3A) and human cerebellum (Figure 3B) were recognized, indicating that SYT14 plays an important role in the cerebellum. These data are in agreement with a scenario in which the *SYT14* mutation causes cerebellar degeneration in this family.

In this study, only one p.Gly484Asp mutation of *SYT14* was identified in association with SCA. Quintero-Rivera et al.[16] previously described a 12-year-old female with cerebral atrophy, absence seizures, developmental delay with a WISC III score of 58 for full IQ, and de novo t(1;3)(q32.1;q25.1) disrupting *SYT14*. Her brain MRI showed diffuse cerebral atrophy, including that of the cerebellar hemisphere and vermis. Although the inheritance modes are different (recessive impact on our family and dominant on the female patient), mild to moderate mental retardation and cerebellar atrophy are common among patients with *SYT14* abnormalities. It will be important to assess the future phenotype of the female patient studied by Quintero-Rivera et al.[16]

Relatively common ARCAs in Japan include ataxia, early-onset; oculomotor apraxia, hypoalbuminemia/ataxia-oculomotor apraxia 1 (EAOH/AOA1 [MIM 208920]); ataxia-oculomotor apraxia 2 (AOA2 [MIM 606002]); spastic ataxia; Charlevoix-Saguenay type (SACS [MIM 270550]); ataxia with isolated vitamin E deficiency (AVED [MIM 277460]); and ataxia-telangiectasia (AT [MIM 208900]). (Friedrich ataxia 1 [FRDA (MIM 229300)] has never been described in the Japanese population.) In this family, patients never showed ocularmotor apraxia, spasticity, peripheral neuropathy, retinal abnormality, immunological abnormality, or other systemic involvements. As an adult-onset type of pure ARCA, SYNE1-related ARCA (also known as spinocerebellar ataxia, autosomal-recessive 8; SCAR8 [MIM 610743]) is found to be caused by mutations of the gene encoding synaptic nuclear envelope protein 1.[22] Furthermore, these patients were not associated with psychomotor retardation. Thus, SYT14-mutated ARCA, described here, should be categorized to a distinct type of ARCA.

SYTs is a large family of transmembrane proteins associated with exocytosis of secretory vesicles (including synaptic vesicles).[23] The mammalian SYT family is composed

of 17 members. SYTs are anchored to the secretory vesicles via a single transmembrane domain (TM) close to its N terminus and have tandem cytoplasmic domains, C2A and C2B.[24] Among SYTs, SYT1 (MIM 185605) is involved in neurotransmitter release and has been intensively studied. The crystal structure of the C2 domains consists of a compact eight-stranded β-barrel with two protruding loops (loops 1 and 3) that form the Ca^{2+}-binding pockets.[25] SYT1 binds three and two Ca^{2+} ions via loops 1 and 3 of C2A and C2B, respectively. Ca^{2+} binding triggers the rapid penetration of the C2 domains into membranes harboring negatively charged phospholipids. Ca^{2+} also promotes SYT1 binding to t-SNAREs (target-membrane-soluble N-ethylmaleimide-sensitive factor attachment protein receptors). SYT1 is a key sensor for evoked and synchronous neurotransmitter release in many classes of neurons.[23] SYT14 also has TM, C2A, and C2B domains, but it has no conserved Ca^{2+}-binding motif that includes the conserved aspartic acid residues in loops 1 and 3 of C2A and C2B.[26] Although the roles of SYTs as Ca^{2+} sensors have been studied extensively, little is known about Ca^{2+}-independent SYTs, which might inhibit the SNARE-catalyzed fusion in both the absence and presence of Ca^{2+}.[27] Recently, Zhang et al.[28] suggested that Ca^{2+}-independent SYT4 (MIM 600103) negatively regulates exocytosis, regardless of its inability to induce Ca^{2+}-dependent exocytosis.

SYT14 has phospholipid-binding activity that is Ca^{2+} independent.[14] The glycine residue mutated in the family is located around the C2B domain loop 1, which plays an important role in binding to phospholipids in SYT1.[25] We confirmed that, compared to the wild-type, the mutation did not alter the binding activity of SYT14 to phospholipids. In an overexpression system, wild-type SYT14 as well as normal variants were distributed in the cytoplasm close to the plasma membrane, showing in-line accumulation along with the membrane. In contrast, the p.Gly484Asp mutant showed a different (reticular) distribution pattern. In the ER, several cotranslational and posttranslational modifications that are required for the correct folding of transmembrane and secretory proteins take place.[29,30] Incompletely folded proteins are generally excluded from ER exit sites.[29] The fact that the p.Gly484Asp was not properly transferred from the ER suggests that the mutant protein might not fold correctly. The lower yield of the mutant protein as compared to the wild-type in the bacterial expression system we performed also supports the improper folding of the mutant. Abnormal distribution in the ER might result in the loss of function of SYT14 or in ER dysfunction.

In conclusion we have shown that SYT14 is localized specifically in Purkinje cells of mouse and human cerebellum. The results strongly support the involvement of SYT14 in the pathogenesis of SCA and are consistent with the atrophy of the cerebellum seen in both patients. A possible relationship between SYTs and neurodegeneration has been suggested previously,[31] and here we provide data that support the idea that disruption of an SYT protein is involved in human neurodegeneration and that exocytosis machinery can be involved in one of the pathomechanisms of neurodegeneration.

Supplemental Data

Supplemental Data include two figures and five tables and can be found with this article online at http://www.cell.com/AJHG/.

Acknowledgments

We would like to thank the patients and their family for their participation in this study. We are indebted to Syu-ichi Hirai (Department of Molecular Biology, Yokohama City University) for providing useful technical information about subcellular fractionation and to Keiko Yamaoka (Kanagawa Rehabilitation Center) for providing brain tissue from the control subject. This work was supported by research grants from the Ministry of Health, Labour, and Welfare (H.S., N. Miyake, and N. Matsumoto), the Japan Science and Technology Agency (N. Matsumoto), a Grant-in-Aid for Scientific Research from the Japan Society for the Promotion of Science (N. Matsumoto), a Grant-in-Aid for Young Scientist from the Japan Society for the Promotion of Science (H.D., N. Miyake, and H.S.) and a grant-in-aid from The Kimi Imai Memorial Foundation for Research of Incurable Neuromuscular Diseases (H.D.).

Received: June 4, 2011
Revised: July 11, 2011
Accepted: July 15, 2011
Published online: August 11, 2011

Web Resources

The URLs for data presented herein are as follows:

Align GVGD, http://agvgd.iarc.fr/
Allen Human brain Atlas, http://human.brain-map.org/
Allen Mouse Brain Atlas, http://mouse.brain-map.org/
HomozygosityMapper, http://www.homozygositymapper.org/
Online Mendelian Inheritance in Man (OMIM), http://www.omim.org/
PolyPhen, http://genetics.bwh.harvard.edu/pph/
PolyPhen2, http://genetics.bwh.harvard.edu/pph2/
SIFT, http://blocks.fhcrc.org/sift/SIFT.html

Rerefences

1. Fogel, B.L., and Perlman, S. (2007). Clinical features and molecular genetics of autosomal recessive cerebellar ataxias. Lancet Neurol. *6*, 245–257.
2. Palau, F., and Espinós, C. (2006). Autosomal recessive cerebellar ataxias. Orphanet J. Rare Dis. *1*, 47.
3. Embiruçu, E.K., Martyn, M.L., Schlesinger, D., and Kok, F. (2009). Autosomal recessive ataxias: 20 types, and counting. Arq. Neuropsiquiatr. *67*, 1143–1156.
4. Anheim, M., Fleury, M., Monga, B., Laugel, V., Chaigne, D., Rodier, G., Ginglinger, E., Boulay, C., Courtois, S., Drouot, N., et al. (2010). Epidemiological, clinical, paraclinical and

molecular study of a cohort of 102 patients affected with autosomal recessive progressive cerebellar ataxia from Alsace, Eastern France: Implications for clinical management. Neurogenetics *11*, 1–12.
5. Manto, M., and Marmolino, D. (2009). Cerebellar ataxias. Curr. Opin. Neurol. *22*, 419–429.
6. Vermeer, S., Hoischen, A., Meijer, R.P., Gilissen, C., Neveling, K., Wieskamp, N., de Brouwer, A., Koenig, M., Anheim, M., Assoum, M., et al. (2010). Targeted next-generation sequencing of a 12.5 Mb homozygous region reveals *ANO10* mutations in patients with autosomal-recessive cerebellar ataxia. Am. J. Hum. Genet. *87*, 813–819.
7. Seelow, D., Schuelke, M., Hildebrandt, F., and Nurnberg, P. (2009). HomozygosityMapper—An interactive approach to homozygosity mapping. Nucleic Acids Res. *37*, W593–W599.
8. Bahlo, M., and Bromhead, C.J. (2009). Generating linkage mapping files from Affymetrix SNP chip data. Bioinformatics *25*, 1961–1962.
9. Gudbjartsson, D.F., Thorvaldsson, T., Kong, A., Gunnarsson, G., and Ingolfsdottir, A. (2005). Allegro version 2. Nat. Genet. *37*, 1015–1016.
10. Li, H., Ruan, J., and Durbin, R. (2008). Mapping short DNA sequencing reads and calling variants using mapping quality scores. Genome Res. *18*, 1851–1858.
11. Gilissen, C., Arts, H.H., Hoischen, A., Spruijt, L., Mans, D.A., Arts, P., van Lier, B., Steehouwer, M., van Reeuwijk, J., Kant, S.G., et al. (2010). Exome sequencing identifies *WDR35* variants involved in Sensenbrenner syndrome. Am. J. Hum. Genet. *87*, 418–423.
12. Tsurusaki, Y., Osaka, H., Hamanoue, H., Shimbo, H., Tsuji, M., Doi, H., Saitsu, H., Matsumoto, N., and Miyake, N. (2011). Rapid detection of a mutation causing X-linked leucoencephalopathy by exome sequencing. J. Med. Genet., in press. Published online March 17, 2011. 10.1136/jmg.2010.083535.
13. Becker, J., Semler, O., Gilissen, C., Li, Y., Bolz, H.J., Giunta, C., Bergmann, C., Rohrbach, M., Koerber, F., Zimmermann, K., et al. (2011). Exome sequencing identifies truncating mutations in human *SERPINF1* in autosomal-recessive osteogenesis imperfecta. Am. J. Hum. Genet. *88*, 362–371.
14. Fukuda, M. (2003). Molecular cloning, expression, and characterization of a novel class of synaptotagmin (Syt XIV) conserved from *Drosophila* to humans. J. Biochem. *133*, 641–649.
15. Adolfsen, B., Saraswati, S., Yoshihara, M., and Littleton, J.T. (2004). Synaptotagmins are trafficked to distinct subcellular domains including the postsynaptic compartment. J. Cell Biol. *166*, 249–260.
16. Quintero-Rivera, F., Chan, A., Donovan, D.J., Gusella, J.F., and Ligon, A.H. (2007). Disruption of a synaptotagmin (*SYT14*) associated with neurodevelopmental abnormalities. Am. J. Med. Genet. A. *143*, 558–563.
17. Michelsen, U., and von Hagen, J. (2009). Isolation of subcellular organelles and structures. Methods Enzymol. *463*, 305–328.
18. Fukuda, M., Kojima, T., and Mikoshiba, K. (1996). Phospholipid composition dependence of Ca^{2+}-dependent phospholipid binding to the C2A domain of synaptotagmin IV. J. Biol. Chem. *271*, 8430–8434.
19. Doi, H., Mitsui, K., Kurosawa, M., Machida, Y., Kuroiwa, Y., and Nukina, N. (2004). Identification of ubiquitin-interacting proteins in purified polyglutamine aggregates. FEBS Lett. *571*, 171–176.
20. Jana, N.R., Tanaka, M., Wang, G., and Nukina, N. (2000). Polyglutamine length-dependent interaction of Hsp40 and Hsp70 family chaperones with truncated N-terminal huntingtin: Their role in suppression of aggregation and cellular toxicity. Hum. Mol. Genet. *9*, 2009–2018.
21. Oyama, F., Miyazaki, H., Sakamoto, N., Becquet, C., Machida, Y., Kaneko, K., Uchikawa, C., Suzuki, T., Kurosawa, M., Ikeda, T., et al. (2006). Sodium channel beta4 subunit: down-regulation and possible involvement in neuritic degeneration in Huntington's disease transgenic mice. J. Neurochem. *98*, 518–529.
22. Gros-Louis, F., Dupré, N., Dion, P., Fox, M.A., Laurent, S., Verreault, S., Sanes, J.R., Bouchard, J.P., and Rouleau, G.A. (2007). Mutations in *SYNE1* lead to a newly discovered form of autosomal recessive cerebellar ataxia. Nat. Genet. *39*, 80–85.
23. McCue, H.V., Haynes, L.P., and Burgoyne, R.D. (2010). The diversity of calcium sensor proteins in the regulation of neuronal function. Cold Spring Harb. Perspect. Biol. *2*, a004085.
24. Bai, J., and Chapman, E.R. (2004). The C2 domains of synaptotagmin—partners in exocytosis. Trends Biochem. Sci. *29*, 143–151.
25. Chapman, E.R. (2008). How does synaptotagmin trigger neurotransmitter release? Annu. Rev. Biochem. *77*, 615–641.
26. Rickman, C., Craxton, M., Osborne, S., and Davletov, B. (2004). Comparative analysis of tandem C2 domains from the mammalian synaptotagmin family. Biochem. J. *378*, 681–686.
27. Bhalla, A., Chicka, M.C., and Chapman, E.R. (2008). Analysis of the synaptotagmin family during reconstituted membrane fusion. Uncovering a class of inhibitory isoforms. J. Biol. Chem. *283*, 21799–21807.
28. Zhang, G., Bai, H., Zhang, H., Dean, C., Wu, Q., Li, J., Guariglia, S., Meng, Q., and Cai, D. (2011). Neuropeptide exocytosis involving synaptotagmin-4 and oxytocin in hypothalamic programming of body weight and energy balance. Neuron *69*, 523–535.
29. Ellgaard, L., and Helenius, A. (2003). Quality control in the endoplasmic reticulum. Nat. Rev. Mol. Cell Biol. *4*, 181–191.
30. Colgan, S.M., Hashimi, A.A., and Austin, R.C. (2011). Endoplasmic reticulum stress and lipid dysregulation. Expert Rev. Mol. Med. *13*, e4.
31. Glavan, G., Schliebs, R., and Zivin, M. (2009). Synaptotagmins in neurodegeneration. Anat. Rec. (Hoboken) *292*, 1849–1862.
32. Schmitz-Hübsch, T., du Montcel, S.T., Baliko, L., Berciano, J., Boesch, S., Depondt, C., Giunti, P., Globas, C., Infante, J., Kang, J.S., et al. (2006). Scale for the assessment and rating of ataxia: Development of a new clinical scale. Neurology *66*, 1717–1720.